

Phonon-mediated decay of an atom in a surface-induced potential

Fam Le Kien,^{1,*} S. Dutta Gupta,^{1,2} and K. Hakuta¹

¹*Department of Applied Physics and Chemistry, University of Electro-Communications, Chofu, Tokyo 182-8585, Japan*

²*School of Physics, University of Hyderabad, Hyderabad, India*

(Received 14 March 2007; published 19 June 2007)

We study phonon-mediated transitions between translational levels of an atom in a surface-induced potential. We present a general master equation governing the dynamics of the translational states of the atom. In the framework of the Debye model, we derive compact expressions for the rates for both upward and downward transitions. Numerical calculations for the transition rates are performed for a deep silica-induced potential allowing for a large number of bound levels as well as free states of a cesium atom. The total absorption rate is shown to be determined mainly by the bound-to-bound transitions for deep bound levels and by bound-to-free transitions for shallow bound levels. Moreover, the phonon emission and absorption processes can be orders of magnitude larger for deep bound levels as compared to the shallow bound ones. We also study various types of transitions from free states. We show that, for thermal atomic cesium with a temperature in the range from 100 μ K to 400 μ K in the vicinity of a silica surface with a temperature of 300 K, the adsorption (free-to-bound decay) rate is about two times larger than the heating (free-to-free upward decay) rate, while the cooling (free-to-free downward decay) rate is negligible.

DOI: 10.1103/PhysRevA.75.062904

PACS number(s): 34.50.Dy, 33.70.Ca

I. INTRODUCTION

Over the past few years, tight confinement of cold atoms has drawn considerable attention. The interest in this area is motivated not only by the fundamental nature of the problem, but also by its potential applications in atom optics and quantum information. A method for microscopic trapping and guiding of individual atoms along a nanofiber has been proposed [1]. Surface-atom quantum electrodynamic effects have constituted another interesting area, where a great deal of work has been carried out. Modification of spontaneous emission of an atom [2] and radiative exchange between two distant atoms [3] mediated by a nanofiber have been investigated. Surface-induced deep potentials have played a major role and have received due attention in recent years. Oria *et al.* have studied various theoretical schemes to load atoms into such potentials [4,5]. A rigorous theory of spontaneous decay of an atom in a surface-induced potential invoking the density-matrix formalism has been developed [6]. The role of interference between the emitted and reflected fields and also the role of transmission into the evanescent modes were identified. Further calculations on the excitation spectrum have been carried out [7]. Bound-to-bound transitions were shown to lead to significant effects like a large red tail of the excitation spectrum as compared to the weak consequences of free-to-bound transitions. A crucial step in this direction was the experimental observation of the excitation spectrum and the channeling of the fluorescent photons along the nanofiber [8], opening up avenues for novel quantum information devices.

In most of the problems involving surface-atom interaction, the macroscopic surface is usually kept at room temperature. Thus the pertinent question that can be asked is

what would be the effect of heating on the cold atoms? It is understood that transfer of heat to the trapped atoms will lead to a change in the occupation probability of the vibrational levels as well as their coherence. Phonon-induced changes in the populations of the vibrational levels have been studied by several groups [5,9,10]. In a nice and compact treatment based on the dyadic Green function and the Fermi golden rule, Henkel *et al.* showed that the effects can be very different depending on the nature of the atomic or molecular species [9]. The time scales for various species were estimated. It should be stressed that the trap considered by Henkel *et al.* was not necessarily a surface trap and misses out on many of the aspects of the surface-atom interaction [9]. Based on the assumption that the surface-atom interaction can be represented by a Morse potential, the phonon-mediated decay was estimated by Oria *et al.* [5]. Their estimate was based on the formalism developed by Gortel *et al.* [10]. However, all the previous theories focus only on the transition rates and thus are not general enough.

In this paper, we study phonon-mediated transitions between vibrational states of an atom in the vicinity of a planar surface. For simplicity, we neglect surface waves and scattering with the lattice. We present a general density-matrix formalism to calculate the phonon-mediated decay of populations as well as the changes in coherence. We derive the relevant master equation for the density matrix of the atom. We emphasize that our density-matrix equation describes the full dynamics of the coupling between trapped atoms and phonons and does not assume any particular form of the trapping potential. Under the Debye approximation, we derive compact expressions for the phonon-mediated decay rates. Numerical calculations are carried out assuming the potential model considered in [4]. In contrast to the previous work, we include a large number of vibrational levels due to the deep surface-atom potential. We show that there can be significant differences in the decay rates when the initial level is chosen as one of the shallow or deep bound levels.

*Also at Institute of Physics and Electronics, Vietnamese Academy of Science and Technology, Hanoi, Vietnam.

We also calculate and analyze the decay rates for various types of transitions from free states.

The paper is organized as follows. In Sec. II we describe the model. In Sec. III we derive the basic dynamical equations for the phonon-mediated decay processes. In Sec. IV we present the results of numerical calculations. Our conclusions are given in Sec. V.

II. DESCRIPTION OF THE MODEL SYSTEM

We assume the whole space to be divided into two regions, namely, the half-space $x < 0$, occupied by a nondispersive nonabsorbing dielectric medium (medium 1), and the half-space $x > 0$, occupied by vacuum (medium 2). We examine a single atom moving in the empty half-space $x > 0$. We assume that the atom is in a fixed internal state $|i\rangle$ with energy $\hbar\omega_i$. Without loss of generality, we assume that the energy of the internal state $|i\rangle$ is zero, i.e., $\omega_i = 0$. We describe the interaction between the atom and the planar surface. We first consider the surface-induced interaction potential and then add the atom-phonon interaction.

A. Surface-induced interaction potential

In this subsection, we describe the interaction between the atom and the surface in the case where thermal vibrations of the surface are absent. The potential energy of the surface-atom interaction is a combination of a long-range van der Waals attraction and a short-range repulsion [11]. Despite a large volume of research on the surface-atom interaction, due to the complexity of surface physics and the lack of data, the actual form of the potential is yet to be ascertained [4,5,9,11,12]. For the purpose of numerical demonstration of our formalism, we choose the following model for the potential [4,11]:

$$U(x) = Ae^{-\alpha x} - \frac{C_3}{x^3}. \quad (1)$$

Here, C_3 is the van der Waals coefficient, while A and α determine the height and range, respectively, of the surface repulsion. The potential parameters C_3 , A , and α depend on the nature of the dielectric and the atom. In numerical calculations, we use the parameters of fused silica, for the dielectric, and the parameters of ground-state atomic cesium, for the atom. The parameters for the interaction between silica and ground-state atomic cesium are theoretically estimated to be $C_3 = 1.56 \text{ kHz } \mu\text{m}^3$, $A = 1.6 \times 10^{18} \text{ Hz}$, and $\alpha = 53 \text{ nm}^{-1}$ [6].

We introduce the notation $\varphi_\nu(x)$ for the eigenfunctions of the center-of-mass motion of the atom in the potential $U(x)$. They are determined by the stationary Schrödinger equation

$$\left[-\frac{\hbar^2}{2m} \frac{d^2}{dx^2} + U(x) \right] \varphi_\nu(x) = \mathcal{E}_\nu \varphi_\nu(x). \quad (2)$$

Here m is the mass of the atom. In the numerical example with atomic cesium, we have $m = 132.9 \text{ a.u.} = 2.21 \times 10^{-25} \text{ kg}$. The eigenvalues \mathcal{E}_ν are the center-of-mass energies of the translational levels of the atom. These eigenvalues

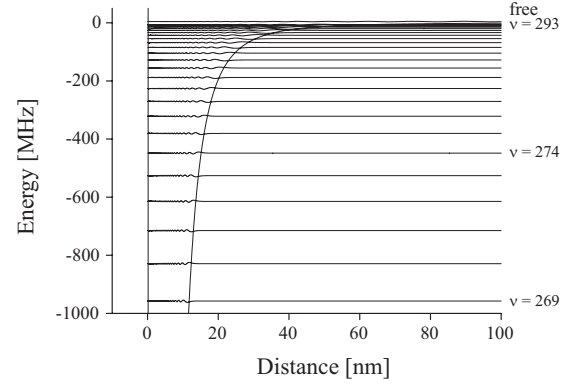


FIG. 1. Energies and wave functions of the center-of-mass motion of an atom in a surface-induced potential. The parameters of the potential are $C_3 = 1.56 \text{ kHz } \mu\text{m}^3$, $A = 1.6 \times 10^{18} \text{ Hz}$, and $\alpha = 53 \text{ nm}^{-1}$. The mass of the atom is $m = 2.21 \times 10^{-25} \text{ kg}$. We plot bound levels with energies in the range from -1 GHz to -5 MHz and also a free state with energy of about 4.25 MHz .

are the shifts of the energies of the translational levels from the energy of the internal state $|i\rangle$. Without loss of generality, we assume that the center-of-mass eigenfunctions $\varphi_\nu(x)$ are real functions, i.e., $\varphi_\nu^*(x) = \varphi_\nu(x)$.

In Fig. 1, we show the potential $U(x)$ and the wave functions $\varphi_\nu(x)$ of a number of bound levels with energies in the range from -1 GHz to -5 MHz . We also plot the wave function of a free state with energy of about 4.25 MHz . In order to have some estimate about the spatial extent of a wave function $\varphi_\nu(x)$, we define a crossing point x_{cross} , which corresponds to the rightmost solution of the equation $U(x) = \mathcal{E}_\nu$. Note that, for shallow levels, the wave function generally peaks close to the point x_{cross} . We plot the eigenvalue modulus $|\mathcal{E}_\nu|$ and the crossing point x_{cross} in Figs. 2(a) and 2(b), respectively. It is clear from the figure that, for ν in the range from 0 to 300, the eigenvalue varies dramatically from about 158 THz to about 322 kHz , while the wave function extends only up to 170 nm .

We introduce the notation $|\nu\rangle = |\varphi_\nu\rangle$ and $\omega_\nu = \mathcal{E}_\nu/\hbar$ for the state vectors and frequencies of translational levels. Then, the Hamiltonian of the atom in the surface-induced potential can be represented in the diagonal form

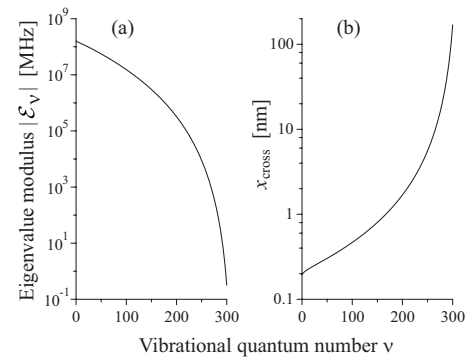


FIG. 2. (a) Eigenvalue modulus $|\mathcal{E}_\nu|$ and (b) crossing point x_{cross} as functions of the vibrational quantum number ν . The parameters used are as in Fig. 1.

$$H_A = \sum_{\nu} \hbar \omega_{\nu} \sigma_{\nu\nu}. \quad (3)$$

Here, $\sigma_{\nu\nu} = |\nu\rangle\langle\nu|$ is the population operator for the translational level ν . We emphasize that the summation over ν includes both the discrete ($\mathcal{E}_{\nu} < 0$) and continuous ($\mathcal{E}_{\nu} > 0$) spectra. The levels ν with $\mathcal{E}_{\nu} < 0$ are called the bound (or vibrational) levels. In such a state, the atom is bound to the surface. It is vibrating, or more exactly, moving back and forth between the walls formed by the van der Waals part and the repulsive part of the potential. The levels ν with $\mathcal{E}_{\nu} > 0$ are called the free (or continuum) levels. The center-of-mass wave functions of the bound states are normalized to unity. The center-of-mass wave functions of the free states are normalized to the delta function of energy.

B. Atom-phonon interaction

In this subsection, we incorporate the thermal vibrations of the solid into the model. Due to the thermal effects, the surface of the dielectric vibrates. The surface-induced potential for the atom is then $U(x-x_s)$, where x_s is the displacement of the surface from the mean position $\langle x_s \rangle = 0$. We approximate the vibrating potential $U(x-x_s)$ by expanding it to the first order in x_s ,

$$U(x-x_s) = U(x) - U'(x)x_s. \quad (4)$$

The first term, $U(x)$, when combined with the kinetic energy $p^2/2m$, yields the Hamiltonian H_A [see Eq. (3)], which leads to the formation of translational levels of the atom. The second term, $-U'(x)x_s$, accounts for the thermal effects in the interaction of the atom with the solid. Note that the quantity $F = -U'(x)$ is the force of the surface upon the atom. Hence the force of the atom upon the surface is $-F = U'(x)$ and, consequently, $U'(x)x_s$ is the work required to displace the surface for a small distance x_s .

In order to describe the displacement x_s of the surface, we use a simple bulk phonon model [10]. For simplicity, we neglect surface waves, which do not change the results in a qualitative way [10,13]. In the framework of the phonon model, only the phonons polarized along the x direction are responsible for the displacement x_s [10]. In the harmonic approximation, we have

$$x_s = \sum_{\mathbf{q}} \left(\frac{\hbar}{2MN\omega_{\mathbf{q}}} \right)^{1/2} (b_{\mathbf{q}} e^{i\mathbf{q}\cdot\mathbf{R}} + b_{\mathbf{q}}^{\dagger} e^{-i\mathbf{q}\cdot\mathbf{R}}). \quad (5)$$

Here, M is the mass of a particle of the solid, N is the particle number density, $\omega_{\mathbf{q}}$ and \mathbf{q} are the frequency and wave vector of the x -polarized acoustic phonons, respectively, $\mathbf{R} = (0, y, z)$ is the lateral component of the position vector (x, y, z) of the atom, and $b_{\mathbf{q}}$ and $b_{\mathbf{q}}^{\dagger}$ are the annihilation and creation phonon operators, respectively. Without loss of generality, we choose $\mathbf{R} = 0$. Meanwhile, the operator U' can be decomposed as $U' = \sum_{\nu\nu'} \sigma_{\nu\nu'} \langle \nu | U' | \nu' \rangle$, where $\sigma_{\nu\nu'} = |\nu\rangle\langle\nu'|$ is the operator for the translational transition $\nu \leftrightarrow \nu'$. Hence the energy term $-U'(x)x_s$ leads to the atom-phonon interaction Hamiltonian [10]

$$H_I = \hbar \sum_{\mathbf{q}} \frac{1}{\sqrt{\omega_{\mathbf{q}}}} S(b_{\mathbf{q}} + b_{\mathbf{q}}^{\dagger}), \quad (6)$$

with

$$S = \sum_{\nu\nu'} g_{\nu\nu'} \sigma_{\nu\nu'}. \quad (7)$$

Here we have introduced the atom-phonon coupling coefficients

$$g_{\nu\nu'} = \frac{F_{\nu\nu'}}{\sqrt{2MN\hbar}}, \quad (8)$$

with

$$F_{\nu\nu'} = - \int_{-\infty}^{\infty} \varphi_{\nu}(x) U'(x) \varphi_{\nu'}(x) dx \quad (9)$$

being the matrix elements for the force of the surface upon the atom. We note that $F_{\nu\nu'} = -m\omega_{\nu\nu'}^2 x_{\nu\nu'}$, where $x_{\nu\nu'} = \langle \nu | x | \nu' \rangle$ and $\omega_{\nu\nu'} = \omega_{\nu} - \omega_{\nu'}$ are the surface-atom dipole matrix element and the translational transition frequency, respectively. Hence the coupling coefficient $g_{\nu\nu'}$ depends on the dipole matrix element $x_{\nu\nu'}$ and the transition frequency $\omega_{\nu\nu'}$. Since $\omega_{\nu\nu} = 0$, we have $g_{\nu\nu} = 0$.

We note that the Hamiltonian of the x -polarized acoustic phonons is given by

$$H_B = \sum_{\mathbf{q}} \hbar \omega_{\mathbf{q}} b_{\mathbf{q}}^{\dagger} b_{\mathbf{q}}. \quad (10)$$

The total Hamiltonian of the atom-phonon system is

$$H = H_A + H_I + H_B. \quad (11)$$

We use the above Hamiltonian to study the phonon-mediated decay of the atom.

III. DYNAMICS OF THE ATOM

In this section, we present the basic equations for the phonon-mediated decay processes. We derive a general master equation for the reduced density operator of the atom in Sec. III A, obtain analytical expressions for the relaxation rates and frequency shifts in Sec. III B, and calculate the rates and the shifts in the framework of the Debye model in Sec. III C.

A. Master equation

In the Heisenberg picture, the equation for the phonon operator $b_{\mathbf{q}}(t)$ is

$$\dot{b}_{\mathbf{q}}(t) = -i\omega_{\mathbf{q}} b_{\mathbf{q}}(t) - \frac{i}{\sqrt{\omega_{\mathbf{q}}}} S(t), \quad (12)$$

which has a solution of the form

$$b_{\mathbf{q}}(t) = b_{\mathbf{q}}(t_0) e^{-i\omega_{\mathbf{q}}(t-t_0)} - iW_{\mathbf{q}}(t). \quad (13)$$

Here, t_0 is the initial time and $W_{\mathbf{q}}$ is given by

$$W_{\mathbf{q}}(t) = \frac{1}{\sqrt{\omega_{\mathbf{q}}}} \int_{t_0}^t e^{-i\omega_{\mathbf{q}}(t-\tau)} S(\tau) d\tau. \quad (14)$$

Consider an arbitrary atomic operator \mathcal{O} which acts only on the atomic states but not on the phonon states. The time evolution of this operator is governed by the Heisenberg equation

$$\frac{\partial \mathcal{O}(t)}{\partial t} = \frac{i}{\hbar} [H_A(t) + H_I(t), \mathcal{O}(t)], \quad (15)$$

which, with account of Eqs. (6) and (13), yields

$$\begin{aligned} \frac{\partial \mathcal{O}(t)}{\partial t} &= \frac{i}{\hbar} [H_A(t), \mathcal{O}(t)] \\ &+ \sum_{\mathbf{q}} \frac{i}{\sqrt{\omega_{\mathbf{q}}}} [S(t), \mathcal{O}(t)] [b_{\mathbf{q}}(t_0) e^{-i\omega_{\mathbf{q}}(t-t_0)} - iW_{\mathbf{q}}(t)] \\ &- \sum_{\mathbf{q}} \frac{i}{\sqrt{\omega_{\mathbf{q}}}} [b_{\mathbf{q}}^\dagger(t_0) e^{i\omega_{\mathbf{q}}(t-t_0)} + iW_{\mathbf{q}}^\dagger(t)] [\mathcal{O}(t), S(t)]. \end{aligned} \quad (16)$$

We assume the initial density of the atom-phonon system to be the direct product state

$$\rho_{\Sigma}(t_0) = \rho(t_0) \rho_B(t_0), \quad (17)$$

with the atom in an arbitrary state $\rho(t_0)$ and the phonons in a thermal state

$$\rho_B(t_0) = Z^{-1} \exp[-H_B(t_0)/k_B T]. \quad (18)$$

Here, Z is the normalization constant and T is the temperature of the phonon bath. For the initial condition (17), the Bogolubov's lemma [14], applied to an arbitrary operator $\Theta(t)$, asserts the following:

$$\langle \Theta(t) b_{\mathbf{q}}(t_0) \rangle = \bar{n}_{\mathbf{q}} \langle [b_{\mathbf{q}}(t_0), \Theta(t)] \rangle, \quad (19)$$

where the mean number of phonons in the mode \mathbf{q} is given by

$$\bar{n}_{\mathbf{q}} = \frac{1}{\exp(\hbar\omega_{\mathbf{q}}/k_B T) - 1}. \quad (20)$$

Let Θ be an atomic operator. We then have the commutation relation $[b_{\mathbf{q}}(t), \Theta(t)] = 0$, which yields

$$[b_{\mathbf{q}}(t_0), \Theta(t)] = i e^{i\omega_{\mathbf{q}}(t-t_0)} [W_{\mathbf{q}}(t), \Theta(t)]. \quad (21)$$

Combining Eq. (19) with Eq. (21) leads to

$$\langle \Theta(t) b_{\mathbf{q}}(t_0) \rangle = i e^{i\omega_{\mathbf{q}}(t-t_0)} \bar{n}_{\mathbf{q}} \langle [W_{\mathbf{q}}(t), \Theta(t)] \rangle. \quad (22)$$

We perform the quantum mechanical averaging for expression (16) and use Eq. (22) to eliminate the phonon operators $b_{\mathbf{q}}(t_0)$ and $b_{\mathbf{q}}^\dagger(t_0)$. The resulting equation can be written as

$$\begin{aligned} \frac{\partial \langle \mathcal{O}(t) \rangle}{\partial t} &= \frac{i}{\hbar} \langle [H_A(t), \mathcal{O}(t)] \rangle + \sum_{\mathbf{q}} \frac{\bar{n}_{\mathbf{q}} + 1}{\sqrt{\omega_{\mathbf{q}}}} \langle [S(t), \mathcal{O}(t)] W_{\mathbf{q}}(t) \rangle \\ &+ W_{\mathbf{q}}^\dagger(t) \langle [\mathcal{O}(t), S(t)] \rangle + \sum_{\mathbf{q}} \frac{\bar{n}_{\mathbf{q}}}{\sqrt{\omega_{\mathbf{q}}}} \langle W_{\mathbf{q}}(t) [\mathcal{O}(t), S(t)] \rangle \\ &+ [S(t), \mathcal{O}(t)] W_{\mathbf{q}}^\dagger(t). \end{aligned} \quad (23)$$

We note that Eq. (23) is exact. It does not contain phonon operators explicitly. The dependence on the phonon operators is hidden in the shift of the time argument τ of the operator $S(\tau)$ in expression (14) for the operator $W_{\mathbf{q}}(t)$.

We now show how the dependence of the operator $W_{\mathbf{q}}(t)$ on the phonon operators can be approximately eliminated. We assume that the atom-phonon coupling coefficients $g_{\nu\nu'}$ are small. The use of the zeroth-order approximation $\sigma_{\nu\nu'}(\tau) = \sigma_{\nu\nu'}(t) e^{i\omega_{\nu\nu'}(\tau-t)}$ in the expression for $S(\tau)$ obtained from Eq. (7) yields

$$S(\tau) = \sum_{\nu\nu'} g_{\nu\nu'} \sigma_{\nu\nu'}(t) e^{i\omega_{\nu\nu'}(\tau-t)}, \quad (24)$$

which is accurate to first order in the coupling coefficients. Inserting Eq. (24) into Eq. (14) gives

$$W_{\mathbf{q}}(t) = \frac{2\pi}{\sqrt{\omega_{\mathbf{q}}}} \sum_{\nu\nu'} g_{\nu\nu'} \sigma_{\nu\nu'}(t) \delta_-(\omega_{\nu\nu'} - \omega_{\mathbf{q}}), \quad (25)$$

where

$$\delta_-(\omega) = \lim_{\epsilon \rightarrow 0} \frac{1}{2\pi} \int_{-\infty}^0 e^{-i(\omega+i\epsilon)\tau} d\tau = \frac{i}{2\pi} \frac{1}{\omega} \mathbf{P} + \frac{1}{2} \delta(\omega). \quad (26)$$

Here, in order to take into account the effect of adiabatic turn-on of interaction, we have added a small positive parameter ϵ to the integral and have used the limit $t_0 \rightarrow -\infty$. Introducing the notation

$$K_{\mathbf{q}} = \frac{W_{\mathbf{q}}}{\sqrt{\omega_{\mathbf{q}}}} = \frac{2\pi}{\omega_{\mathbf{q}}} \sum_{\nu\nu'} g_{\nu\nu'} \sigma_{\nu\nu'} \delta_-(\omega_{\nu\nu'} - \omega_{\mathbf{q}}), \quad (27)$$

we can rewrite Eq. (23) in the form

$$\begin{aligned} \frac{\partial \langle \mathcal{O}(t) \rangle}{\partial t} &= \frac{i}{\hbar} \langle [H_A(t), \mathcal{O}(t)] \rangle + \sum_{\mathbf{q}} (\bar{n}_{\mathbf{q}} + 1) \langle [S(t), \mathcal{O}(t)] K_{\mathbf{q}}(t) \rangle \\ &+ K_{\mathbf{q}}^\dagger(t) \langle [\mathcal{O}(t), S(t)] \rangle + \sum_{\mathbf{q}} \bar{n}_{\mathbf{q}} \langle K_{\mathbf{q}}(t) [\mathcal{O}(t), S(t)] \rangle \\ &+ [S(t), \mathcal{O}(t)] K_{\mathbf{q}}^\dagger(t). \end{aligned} \quad (28)$$

In order to examine the time evolution of the reduced density operator $\rho(t)$ of the atom in the Schrödinger picture, we use the relation $\langle \mathcal{O}(t) \rangle = \text{Tr}[\mathcal{O}(t) \rho(0)] = \text{Tr}[\mathcal{O}(0) \rho(t)]$, transform to arrange the operator $\mathcal{O}(0)$ at the first position in each operator product, and eliminate $\mathcal{O}(0)$. Then, we obtain the Liouville master equation

$$\begin{aligned} \frac{\partial \rho(t)}{\partial t} = & -\frac{i}{\hbar} [H_A, \rho(t)] + \sum_{\mathbf{q}} (\bar{n}_{\mathbf{q}} + 1) \{ [K_{\mathbf{q}} \rho(t), S] + [S, \rho(t) K_{\mathbf{q}}^\dagger] \} \\ & + \sum_{\mathbf{q}} \bar{n}_{\mathbf{q}} \{ [S, \rho(t) K_{\mathbf{q}}] + [K_{\mathbf{q}}^\dagger \rho(t), S] \}. \end{aligned} \quad (29)$$

Equations (28) and (29) are valid to second order in the coupling coefficients. These equations allow us to study the time evolution and dynamical characteristics of the atom interacting with the thermal phonon bath. We note that Eq. (29) is a particular form of Zwanzig's generalized master equation, which can be obtained by the projection operator method [15].

B. Relaxation rates and frequency shifts

We use Eq. (29) to derive an equation for the matrix elements $\rho_{jj'} = \langle j | \rho | j' \rangle$ of the reduced density operator of the atom. The result is

$$\begin{aligned} \frac{\partial \rho_{jj'}}{\partial t} = & -i \omega_{jj'} \rho_{jj'} + \sum_{vv'} (\gamma_{jj' vv'}^e + \gamma_{jj' vv'}^a) \rho_{vv'} \\ & - \sum_v [(\gamma_{jv}^e + \gamma_{jv}^a) \rho_{vj'} + (\gamma_{j'v}^{e*} + \gamma_{j'v}^{a*}) \rho_{jv}], \end{aligned} \quad (30)$$

where the coefficients

$$\begin{aligned} \gamma_{jj' vv'}^e = & 2\pi \sum_{\mathbf{q}} \frac{\bar{n}_{\mathbf{q}} + 1}{\omega_{\mathbf{q}}} g_{jv} g_{j' v'} [\delta_-(\omega_{vj} - \omega_{\mathbf{q}}) + \delta_+(\omega_{v' j'} - \omega_{\mathbf{q}})], \\ \gamma_{jv}^e = & 2\pi \sum_{\mathbf{q}} \frac{\bar{n}_{\mathbf{q}} + 1}{\omega_{\mathbf{q}}} g_{j\mu} g_{v\mu} \delta_-(\omega_{v\mu} - \omega_{\mathbf{q}}) \end{aligned} \quad (31)$$

and

$$\begin{aligned} \gamma_{jj' vv'}^a = & 2\pi \sum_{\mathbf{q}} \frac{\bar{n}_{\mathbf{q}}}{\omega_{\mathbf{q}}} g_{jv} g_{j' v'} [\delta_-(\omega_{j' v'} - \omega_{\mathbf{q}}) + \delta_+(\omega_{jv} - \omega_{\mathbf{q}})], \\ \gamma_{jv}^a = & 2\pi \sum_{\mathbf{q}} \frac{\bar{n}_{\mathbf{q}}}{\omega_{\mathbf{q}}} g_{j\mu} g_{v\mu} \delta_+(\omega_{\mu v} - \omega_{\mathbf{q}}) \end{aligned} \quad (32)$$

are the decay parameters associated with the phonon emission and absorption, respectively. Here, the notation $\delta_+(\omega) = \delta_-^*(\omega)$ has been used.

Equation (30) describes phonon-induced variations in the populations and coherences of the translational levels of the atom. We analyze the characteristics of the relaxation processes. For simplicity of mathematical treatment, we first consider only transitions from discrete levels. The equation for the diagonal matrix element ρ_{jj} for a discrete level j can be written in the form

$$\begin{aligned} \frac{\partial \rho_{jj}}{\partial t} = & \sum_v (\gamma_{jj vv}^e + \gamma_{jj vv}^a) \rho_{vv} - (\gamma_{jj}^e + \gamma_{jj}^a + \text{c.c.}) \rho_{jj} \\ & + \text{off-diagonal terms.} \end{aligned} \quad (33)$$

When the off-diagonal terms are neglected, Eq. (33) reduces to a simple rate equation. It is clear from Eq. (33) that the

rate for the downward transition from an upper level l to a lower level k ($k < l$) is

$$R_{kl}^e = \gamma_{kkll}^e = 2\pi \sum_{\mathbf{q}} \frac{\bar{n}_{\mathbf{q}} + 1}{\omega_{\mathbf{q}}} g_{lk}^2 \delta(\omega_{lk} - \omega_{\mathbf{q}}), \quad (34)$$

while the rate for the upward transition from a lower level k to an upper level l ($l > k$) is

$$R_{lk}^a = \gamma_{llkk}^a = 2\pi \sum_{\mathbf{q}} \frac{\bar{n}_{\mathbf{q}}}{\omega_{\mathbf{q}}} g_{lk}^2 \delta(\omega_{lk} - \omega_{\mathbf{q}}). \quad (35)$$

Equations (34) and (35) are in agreement with the results of Gortel *et al.* [10], obtained by using the Fermi golden rule. We note that R_{kl}^e and R_{lk}^a with $l \leq k$ are mathematically equal to zero because they have no physical meaning. For convenience, we introduce the notation $R_{lk} = R_{lk}^e$, R_{lk}^a , or 0 for $l < k$, $l > k$, or $l = k$, respectively. It is clear that the off-diagonal coefficients R_{lk} , with $l \neq k$, are the rates of the transitions from k to l . However, the diagonal coefficients R_{kk} have no physical meaning and are mathematically equal to zero.

As seen from Eq. (33), the phonon-mediated depletion rate of a level k is $\Gamma_{kk} = 2 \text{Re}(\gamma_{kk}^e + \gamma_{kk}^a)$. The explicit expression for this rate is

$$\begin{aligned} \Gamma_{kk} = & 2\pi \sum_{\mathbf{q}, \mu} \frac{\bar{n}_{\mathbf{q}} + 1}{\omega_{\mathbf{q}}} g_{k\mu}^2 \delta(\omega_{k\mu} - \omega_{\mathbf{q}}) \\ & + 2\pi \sum_{\mathbf{q}, \mu} \frac{\bar{n}_{\mathbf{q}}}{\omega_{\mathbf{q}}} g_{\mu k}^2 \delta(\omega_{\mu k} - \omega_{\mathbf{q}}). \end{aligned} \quad (36)$$

We note that $\Gamma_{kk} = \sum_{\mu} (R_{\mu k}^e + R_{\mu k}^a) = \sum_{\mu} R_{\mu k}$. We can write $\Gamma_{kk} = \Gamma_{kk}^e + \Gamma_{kk}^a$, where

$$\Gamma_{kk}^e = \sum_{\mu < k} R_{\mu k}^e \quad (37)$$

and

$$\Gamma_{kk}^a = \sum_{\mu > k} R_{\mu k}^a \quad (38)$$

are the contributions due to downward transitions (phonon emission) and upward transitions (phonon absorption), respectively. We note that, in Eqs. (36)–(38), the summation over μ can be extended to cover not only the discrete levels but also the continuum levels.

Furthermore, the equation for the off-diagonal matrix element ρ_{lk} for a pair of discrete levels l and k can be written in the form $\partial \rho_{lk} / \partial t = -(i\omega_{lk} + \gamma_{ll}^e + \gamma_{ll}^a + \gamma_{kk}^{e*} + \gamma_{kk}^{a*}) \rho_{lk} + \dots$, or, equivalently,

$$\frac{\partial \rho_{lk}}{\partial t} = -i(\omega_{lk} + \Delta_{lk} - i\Gamma_{lk}) \rho_{lk} + \dots \quad (39)$$

Here the frequency shift Δ_{lk} is given by

$$\Delta_{lk} = \sum_{\mathbf{q}\mu} \frac{\bar{n}_{\mathbf{q}} + 1}{\omega_{\mathbf{q}}} \left(\frac{g_{l\mu}^2}{\omega_{l\mu} - \omega_{\mathbf{q}}} + \frac{g_{\mu k}^2}{\omega_{\mu k} + \omega_{\mathbf{q}}} \right) + \sum_{\mathbf{q}\mu} \frac{\bar{n}_{\mathbf{q}}}{\omega_{\mathbf{q}}} \left(\frac{g_{l\mu}^2}{\omega_{l\mu} + \omega_{\mathbf{q}}} + \frac{g_{\mu k}^2}{\omega_{\mu k} - \omega_{\mathbf{q}}} \right), \quad (40)$$

while the coherence decay rate Γ_{lk} is expressed as

$$\Gamma_{lk} = \pi \sum_{\mathbf{q}\mu} \frac{\bar{n}_{\mathbf{q}} + 1}{\omega_{\mathbf{q}}} [g_{l\mu}^2 \delta(\omega_{l\mu} - \omega_{\mathbf{q}}) + g_{\mu k}^2 \delta(\omega_{\mu k} - \omega_{\mathbf{q}})] + \pi \sum_{\mathbf{q}\mu} \frac{\bar{n}_{\mathbf{q}}}{\omega_{\mathbf{q}}} [g_{\mu l}^2 \delta(\omega_{\mu l} - \omega_{\mathbf{q}}) + g_{\mu k}^2 \delta(\omega_{\mu k} - \omega_{\mathbf{q}})]. \quad (41)$$

When we set $l=k$ in Eq. (40), we find $\Delta_{kk}=0$. When we set $l=k$ in Eq. (41), we recover Eq. (36). We note that $\Gamma_{lk} = \sum_{\mu} (R_{\mu l}^e + R_{\mu k}^e + R_{\mu l}^a + R_{\mu k}^a)/2 = \sum_{\mu} (R_{\mu l} + R_{\mu k})/2$. Comparison between Eqs. (41) and (36) yields the relation $\Gamma_{lk} = (\Gamma_{ll} + \Gamma_{kk})/2$. We can also write $\Gamma_{lk} = \Gamma_{lk}^e + \Gamma_{lk}^a$, where $\Gamma_{lk}^e = \sum_{\mu} (R_{\mu l}^e + R_{\mu k}^e)/2$ and $\Gamma_{lk}^a = \sum_{\mu} (R_{\mu l}^a + R_{\mu k}^a)/2$ are the contributions due to downward transitions (phonon emission) and upward transitions (phonon absorption), respectively. We note that, in Eqs. (40) and (41), the summation over μ can be extended to cover not only the discrete levels but also the continuum levels.

We now discuss phonon-mediated transitions from continuum (free) levels. We start by considering free-to-bound transitions. For a continuum level f with energy $\mathcal{E}_f > 0$, the center-of-mass wave function $\varphi_f(x)$ is normalized per unit energy. In this case, the quantity R_{vf} becomes the density of the transition rate. A free level f can be approximated by a level of a quasicontinuum [16]. A discretization of the continuum can be realized by using a large box of length L with reflecting boundary conditions [17]. We label E_n the energies of the eigenstates in the box and $\phi_n(x)$ the corresponding wave functions. Note that such states are standing-wave states [16,17]. The relation between a quasicontinuum-state wave function $\phi_{n_f}(x)$, normalized to unity in the box, and the corresponding continuum-state wave function $\varphi_f(x)$, normalized per unit energy, with equal energies $E_{n_f} = \mathcal{E}_f$, is [17]

$$\varphi_f(x) \equiv \left[\frac{\partial E_{n_f}}{\partial n_f} \right]^{-1/2} \phi_{n_f}(x) \equiv \left(\frac{L}{\pi \hbar} \right)^{1/2} \left(\frac{m}{2E_{n_f}} \right)^{1/4} \phi_{n_f}(x). \quad (42)$$

Consequently, for a single atom initially prepared in the quasicontinuum standing-wave state $|n_f\rangle = |\phi_{n_f}\rangle$, the rate for the transition to an arbitrary bound state $|\nu\rangle$ is approximately given by

$$G_{\nu f} = \frac{\pi \hbar}{L} v_f R_{\nu f}, \quad (43)$$

where $v_f = (2\mathcal{E}_f/m)^{1/2}$ is the velocity of the atom in the initial continuum standing-wave state $|f\rangle$. The phonon-mediated free-to-bound decay rate (adsorption rate) is then given by

$$G_f = \sum_{\nu} G_{\nu f}, \quad (44)$$

where the summation includes only bound levels. It is clear from Eq. (43) that, in the continuum limit $L \rightarrow \infty$, the rate $G_{\nu f}$ tends to zero. This is because a free atom can be anywhere in free space and therefore the effect of phonons on a single free atom is negligible.

In order to get deeper insight into the free-to-bound transition rate density $R_{\nu f}$, we consider a macroscopic atomic ensemble in the thermodynamic limit [16]. Suppose that there are N_0 atoms in a volume with a large length L and a transverse cross section area S_0 . Assume that all the atoms are in the same quasicontinuum state $|n_f\rangle$ and interact with the dielectric independently. The rate for the transitions of the atoms from the quasicontinuum state $|n_f\rangle$ to an arbitrary bound state $|\nu\rangle$, defined as the time derivative of the number of atoms in the state $|\nu\rangle$, is $D_{\nu f} = N_0 G_{\nu f}$. In order to get the rate for the continuum state $|f\rangle$, we need to take the thermodynamical limit, where $L \rightarrow \infty$ and $N_0 \rightarrow \infty$ but N_0/L remains constant. Then, the rate for the transitions of the atoms from the continuum state $|f\rangle$ to an arbitrary bound state $|\nu\rangle$ is given by $D_{\nu f} = \pi \hbar \rho_0 S_0 v_f R_{\nu f} = 2\pi \hbar \mathcal{N}_f R_{\nu f}$. Here, $\rho_0 = N_0/LS_0$ is the atom number density and $\mathcal{N}_f = \rho_0 S_0 v_f/2$ is the number of atoms incident into the dielectric surface per unit time. It is clear that the transition rate $D_{\nu f}$ is proportional to the incidence rate \mathcal{N}_f as well as the transition rate density $R_{\nu f}$. We emphasize that $D_{\nu f}$ is a characteristic for a macroscopic atomic ensemble in the thermodynamic limit while $G_{\nu f}$ is a measure for a single atom. When the length of the box, L , and the number of atoms, N_0 , are finite, the dynamics of the atoms cannot be described by the free-to-bound rate $D_{\nu f}$ directly. Instead, we must use the transition rate per atom $G_{\nu f} = D_{\nu f}/N_0$, which depends on the length L of the box that contains the free atoms [see Eq. (43)].

In a thermal gas, the atoms have different velocities and, therefore, different energies. For a thermal Maxwell-Boltzmann gas with temperature T_0 , the distribution of the kinetic energy \mathcal{E}_f of the atomic center-of-mass motion along the x direction is

$$P(\mathcal{E}_f) = \frac{1}{\sqrt{\pi k_B T_0}} \frac{e^{-\mathcal{E}_f/k_B T_0}}{\sqrt{\mathcal{E}_f}}. \quad (45)$$

The transition rate to an arbitrary bound state $|\nu\rangle$ is then given by $G_{\nu T_0} = \int_0^\infty G_{\nu f} P(\mathcal{E}_f) d\mathcal{E}_f$, i.e.,

$$G_{\nu T_0} = \frac{\lambda_D}{L} \int_0^\infty e^{-\mathcal{E}_f/k_B T_0} R_{\nu f} d\mathcal{E}_f, \quad (46)$$

where $\lambda_D = (2\pi \hbar^2 / m k_B T_0)^{1/2}$ is the thermal de Broglie wavelength. The phonon-mediated free-to-bound decay rate (adsorption rate) is given by

$$G_{T_0} = \sum_{\nu} G_{\nu T_0} = \int_0^\infty G_f P(\mathcal{E}_f) d\mathcal{E}_f. \quad (47)$$

In the above equation, the summation over ν includes only bound levels. Note that Eq. (46) is in qualitative agreement with the results of Refs. [5,16].

It is easy to extend the above results to the case of free-to-free transitions. Indeed, it can be shown that the density of the rate for the transition from a quasicontinuum state $|n_f\rangle$, which corresponds to a free state $|f\rangle$, to a different free state $|f'\rangle$ is given by

$$Q_{f'f} = \frac{\pi\hbar}{L} v_f R_{f'f}. \quad (48)$$

For convenience, we introduce the notation $Q_{f'f}^e = Q_{f'f}$ or 0 for $\mathcal{E}_{f'} < \mathcal{E}_f$ or $\mathcal{E}_{f'} \geq \mathcal{E}_f$, respectively, and $Q_{f'f}^a = Q_{f'f}$ or 0 for $\mathcal{E}_{f'} > \mathcal{E}_f$ or $\mathcal{E}_{f'} \leq \mathcal{E}_f$, respectively. Then, we have $Q_{f'f} = Q_{f'f}^e$ 0, or $Q_{f'f}^a$ for $\mathcal{E}_{f'} < \mathcal{E}_f$, $\mathcal{E}_{f'} = \mathcal{E}_f$, or $\mathcal{E}_{f'} > \mathcal{E}_f$, respectively. The downward (phonon-emission) and upward (phonon-absorption) free-to-free decay rates for the free state $|f\rangle$ are given by

$$Q_f^e = \int_0^{\mathcal{E}_f} Q_{f'f}^e d\mathcal{E}_{f'} \quad (49)$$

and

$$Q_f^a = \int_{\mathcal{E}_f}^{\infty} Q_{f'f}^a d\mathcal{E}_{f'}, \quad (50)$$

respectively. The total free-to-free decay rate for the free state $|f\rangle$ is $Q_f = Q_f^e + Q_f^a = \int_0^{\infty} Q_{f'f} d\mathcal{E}_{f'}$.

For a thermal gas, we need to replace the transition rate density $Q_{f'f}$ and the decay rate Q_f by $Q_{f'T_0}$ $= \int_0^{\infty} Q_{f'f} P(\mathcal{E}_f) d\mathcal{E}_f$ and $Q_{T_0} = \int_0^{\infty} Q_f P(\mathcal{E}_f) d\mathcal{E}_f$, respectively, which are the averages of $Q_{f'f}$ and Q_f , respectively, with respect to the energy distribution $P(\mathcal{E}_f)$ of the initial state. Like in the other cases, we have $Q_{f'T_0} = Q_{f'T_0}^e + Q_{f'T_0}^a$ and $Q_{T_0} = Q_{T_0}^e + Q_{T_0}^a$, where

$$Q_{f'T_0}^e = \int_{\mathcal{E}_{f'}}^{\infty} Q_{f'f}^e P(\mathcal{E}_f) d\mathcal{E}_f, \quad (51)$$

$$Q_{f'T_0}^a = \int_0^{\mathcal{E}_{f'}} Q_{f'f}^a P(\mathcal{E}_f) d\mathcal{E}_f$$

are the downward and upward transition rate densities and

$$Q_{T_0}^e = \int_0^{\infty} Q_f^e P(\mathcal{E}_f) d\mathcal{E}_f, \quad (52)$$

$$Q_{T_0}^a = \int_0^{\infty} Q_f^a P(\mathcal{E}_f) d\mathcal{E}_f$$

are the downward and upward decay rates. The thermal decay rates $Q_{T_0}^e$ and $Q_{T_0}^a$ describe the cooling and heating processes, respectively. It can be easily shown that $Q_{T_0}^e < Q_{T_0}^a$, $Q_{T_0}^e > Q_{T_0}^a$, and $Q_{T_0}^e = Q_{T_0}^a$ when $T_0 < T$, $T_0 > T$, and $T_0 = T$, respectively. The relation $Q_{T_0}^e < Q_{T_0}^a$ ($Q_{T_0}^e > Q_{T_0}^a$), obtained for $T_0 < T$ ($T_0 > T$), indicates the dominance of heating (cooling) of free atoms by the surface.

C. Relaxation rates and frequency shifts in the framework of the Debye model

In order to get insight into the relaxation rates and frequency shifts, we approximate them using the bulk Debye model for phonons. In this model, the phonon frequency ω_q is related to the phonon wave number q as $\omega_q = vq$, where v is the sound velocity. Furthermore, the summation over the first Brillouin zone is replaced by an integral over a sphere of radius $q_D = (6\pi^2 N/V)^{1/3}$, where V is the volume of the solid. The Debye frequency and the Debye temperature are given by $\omega_D = vq_D$ and $T_D = \hbar\omega_D/k_B$, respectively. For fused silica, we have $v = 5.96$ km/s, $N/V = 2.2$ g/cm³, and $M = 9.98 \times 10^{-26}$ kg [18]. Using these parameters, we find $q_D = 109.29 \times 10^6$ cm⁻¹, $\omega_D = 10.4$ THz, and $T_D = 498$ K. In order to perform the summation over phonon states in the framework of the Debye model, we invoke the thermodynamic limit, i.e., replace

$$\sum_{\mathbf{q}} \dots = \frac{V}{8\pi^3} \int_{|\mathbf{q}| \leq q_D} \dots d\mathbf{q} = \frac{3N}{\omega_D^3} \int_0^{\omega_D} \dots \omega_q^2 d\omega_q. \quad (53)$$

Then, for transitions between an upper level l and a lower level k , where $0 < \omega_{lk} < \omega_D$, Eqs. (34) and (35) yield

$$R_{kl}^e = \frac{3\pi}{M\hbar\omega_D^3} (\bar{n}_{lk} + 1) \omega_{lk} F_{lk}^2 \quad (54)$$

and

$$R_{lk}^a = \frac{3\pi}{M\hbar\omega_D^3} \bar{n}_{lk} \omega_{lk} F_{lk}^2. \quad (55)$$

Here, \bar{n}_{lk} is given by Eq. (20) with ω_q replaced by ω_{lk} . We emphasize that, according to Eqs. (54) and (55), the phonon-emission rate R_{kl}^e and the phonon-absorption rate R_{lk}^a depend not only on the matrix element F_{lk} of the force but also on the translational transition frequency ω_{lk} . The frequency dependences of the transition rates are comprised of the frequency dependences of the mean phonon number \bar{n}_{lk} , the phonon mode density $3N\omega_{lk}^2/\omega_D^3$, and the matrix element $F_{lk} = -U'_{lk} = -m\omega_{lk}^2 x_{lk}$ of the force. An additional factor comes from the presence of the phonon frequency in Eq. (5) for the surface displacement and, consequently, in the atom-phonon interaction Hamiltonian (6). It is clear that an increase in the phonon frequency leads to a decrease in the mean phonon number and an increase in the phonon mode density. The matrix element of the force usually first increases and then decreases with increasing transition frequency. Due to the existence of several competing factors, the frequency dependences of the transition rates are rather complicated. They usually first increase and then decrease with increasing transition frequency. We note that, for transitions with $\omega_{lk} > \omega_D$, we have $R_{kl}^e = R_{lk}^a = 0$.

We conclude this section by noting that the use of Eq. (53) in Eq. (40) yields the frequency shift

$$\Delta_{lk} = \Delta_{lk}^{(0)} + \Delta_{lk}^{(T)}, \quad (56)$$

where

$$\Delta_{lk}^{(0)} = \frac{3}{2M\hbar\omega_D^3} \sum_{\mu} \int_0^{\omega_D} \left(\frac{F_{l\mu}^2}{\omega_{l\mu} - \omega} + \frac{F_{\mu k}^2}{\omega_{\mu k} + \omega} \right) \omega d\omega \quad (57)$$

and

$$\Delta_{lk}^{(T)} = \frac{3}{M\hbar\omega_D^3} \sum_{\mu} \int_0^{\omega_D} \left(\frac{\omega_{l\mu} F_{l\mu}^2}{\omega_{l\mu}^2 - \omega^2} + \frac{\omega_{\mu k} F_{\mu k}^2}{\omega_{\mu k}^2 - \omega^2} \right) \bar{n}_{\omega} \omega d\omega \quad (58)$$

are the zero- and finite-temperature contributions, respectively. In Eq. (58), \bar{n}_{ω} is given by Eq. (20) with ω_q replaced by ω .

IV. NUMERICAL RESULTS AND DISCUSSIONS

In this section, we present the numerical results based on the analytical expressions derived in the previous section for the phonon-mediated relaxation rates of the translational levels of the atom. In particular, we use Eqs. (54) and (55), obtained in the framework of the Debye model, for our numerical calculations. We consider transitions from bound states as well as free states. The transitions from bound states to other translational levels occur in the case where the atom is initially already adsorbed or trapped near the surface. The transitions from free states to other translational levels occur in the processes of adsorbing, heating, and cooling of free atoms by the surface. Due to the difference in physics of the initial situations, we study the transitions from bound and free states separately.

A. Transitions from bound states

We start from a given bound level and calculate the rates of phonon-mediated atomic transitions, both downward and upward. The profiles of the phonon-emission (downward-transition) rate $R_{\nu',\nu}^e$ [see Eq. (54)] and the phonon-absorption (upward-transition) rate $R_{\nu',\nu}^a$ [see Eq. (55)] are shown in Figs. 3 and 4, respectively. The upper (lower) part of each of these figures corresponds to the case of the initial level $\nu = 280$ ($\nu = 120$), with energy $\mathcal{E}_{\nu} = -156$ MHz ($\mathcal{E}_{\nu} = -8.4$ THz). The left (right) panel of Fig. 4 corresponds to bound-to-bound (bound-to-free) upward transitions. The temperature of the surface is assumed to be $T = 300$ K. As seen from Figs. 3 and 4, the transition rates have pronounced localized profiles. Due to the competing effects of the mean phonon number, the phonon mode density, and the matrix element of the force, the transition rates usually first increase and then decrease with increasing transition frequency. It is clear from a comparison of Figs. 3(a) and 3(b) and also a comparison of Figs. 4(a) and 4(b) that transitions from shallow levels have probabilities orders of magnitude lower than those from deeper levels. The main reason is that the wave functions of the shallow states are spread further away from the surface than those for the deep states. Due to this difference, the effects of the surface vibrations are weaker for the shallow levels than for the deep levels. Another pertinent feature that should be noted from the figure is the following: Since transition frequencies involved are large, they may overshoot the Debye frequency $\omega_D = 10.4$ THz, leading to a cutoff on the

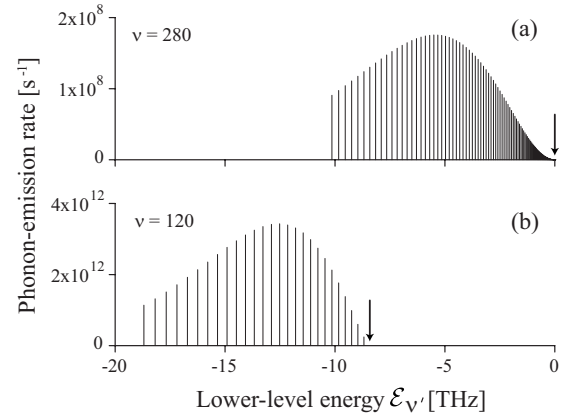


FIG. 3. Phonon-emission rates $R_{\nu',\nu}^e$ from the vibrational levels (a) $\nu = 280$ and (b) $\nu = 120$ to other levels ν' as functions of the lower-level energy $\mathcal{E}_{\nu'}$. The arrows mark the initial states. The parameters of the solid are $M = 9.98 \times 10^{-26}$ kg and $\omega_D = 10.4$ THz. The temperature of the phonon bath is $T = 300$ K. Other parameters are as in Fig. 1.

lower (higher) side of the frequency axis for the emission (absorption) curve.

In order to see the overall effect of the individual transition rates shown above, we add them up. First we examine the phonon-absorption rates of bound levels. The total phonon-absorption rate $\Gamma_{\nu\nu'}^a$ of a bound level ν is the sum of the individual absorption rates $R_{\mu\nu}^a$ over all the upper levels μ , both bound and free [see Eq. (38)]. We plot in Fig. 5 the contributions to $\Gamma_{\nu\nu'}^a$ from two types of transitions, bound-to-bound and bound-to-free (desorption) transitions. The solid curve of the figure shows that the bound-to-bound phonon-absorption rate is large (above 10^{10} s $^{-1}$) for deep and intermediate levels. However, it reduces dramatically with increasing ν in the region of large ν and becomes very small

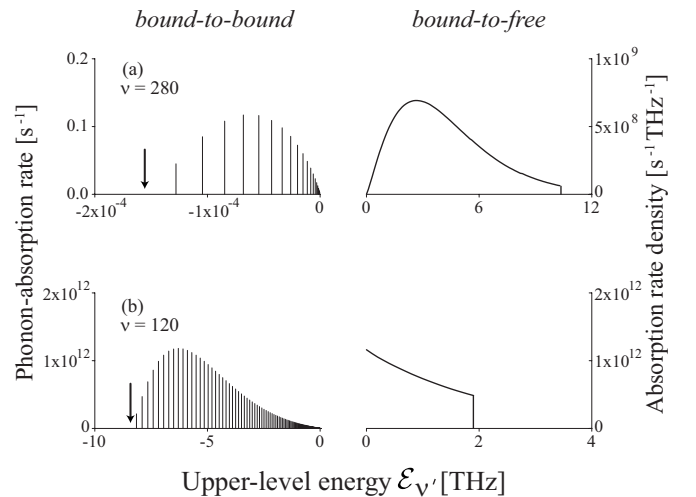


FIG. 4. Phonon-absorption rates $R_{\nu',\nu}^a$ from the vibrational levels (a) $\nu = 280$ and (b) $\nu = 120$ to other levels ν' as functions of the upper-level energy $\mathcal{E}_{\nu'}$. The left (right) panel in each row corresponds to bound-to-bound (bound-to-free) transitions. The arrows mark the initial states. The parameters used are as in Fig. 3. The temperature of the phonon bath is $T = 300$ K.

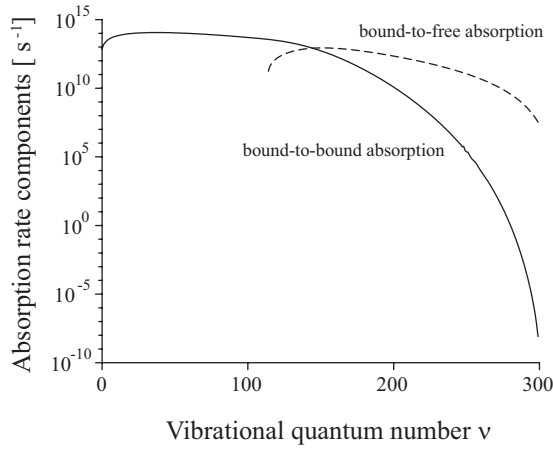


FIG. 5. Contributions of bound-to-bound (solid curve) and bound-to-free (dashed curve) transitions to the total phonon-absorption rate $\Gamma^a_{\nu\nu}$ versus the vibrational quantum number ν of the initial level. The parameters used are as in Fig. 3. The temperature of the phonon bath is $T=300$ K.

(below 10^{-5} s^{-1}) for shallow levels. Meanwhile, the dashed curve of Fig. 5 shows that the bound-to-free phonon-absorption rate (i.e., the desorption rate) is zero for deep levels, since the energy required for the transition is greater than the Debye energy [5]. However, the desorption rate is substantial (above 10^5 s^{-1}) for intermediate and shallow levels. Thus the total phonon-absorption rate $\Gamma^a_{\nu\nu}$ is mainly determined by the bound-to-bound transitions in the case of deep levels and by the bound-to-free transitions in the case of shallow levels. One of the reasons for the dramatic reduction of the bound-to-bound phonon-absorption rate in the region of shallow levels is that the number of upper bound levels μ becomes small. The second reason is that the frequency of each individual transition becomes small, leading to a decrease of the phonon mode density. The third reason is that the center-of-mass wave functions of shallow levels are

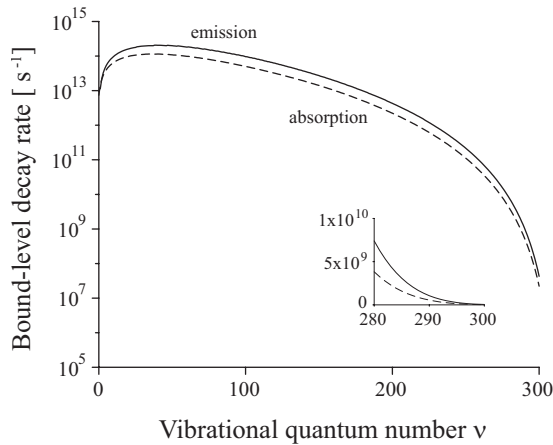


FIG. 6. Phonon-emission decay rate $\Gamma^e_{\nu\nu}$ (solid lines) and phonon-absorption decay rate $\Gamma^a_{\nu\nu}$ (dashed lines) of a bound level as functions of the vibrational quantum number ν . The inset shows the rates in the linear scale to highlight the differences in the dissociation limit. The parameters used are as in Fig. 3. The temperature of the phonon bath is $T=300$ K.

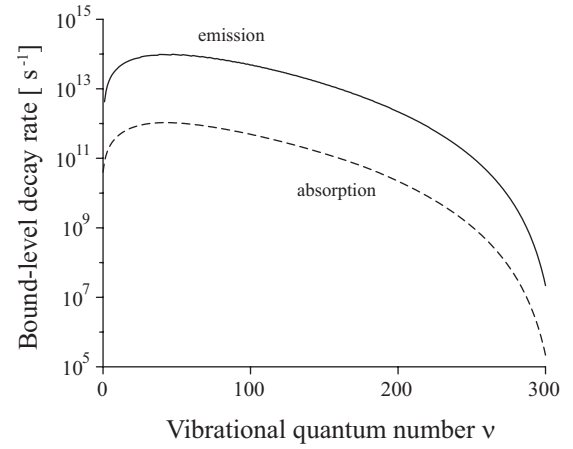


FIG. 7. Same as in Fig. 6 except that $T=30$ K.

spread far away from the surface, leading to a reduction of the effect of phonons on the atom.

Unlike the bound-to-bound phonon-absorption rate, the bound-to-free phonon-absorption rate is substantial in the region of shallow levels. This is because the free-state spectrum is continuous and the range of the bound-to-free transition frequency can be large (up to the Debye frequency $\omega_D=10.4$ THz). The gradual reduction of the bound-to-free phonon-absorption rate in the region of shallow levels is mainly due to the reduction of the time that the atom spends in the proximity of the surface.

The total phonon-emission rate $\Gamma^e_{\nu\nu}$ [see Eq. (37)] and the total phonon-absorption rate $\Gamma^a_{\nu\nu}$ [see Eq. (38)] are shown in Fig. 6 by the solid and dashed curves, respectively. It is clear from the figure that the emission is comparable to but slightly stronger than the absorption. Such a dominance is due to the fact that phonon emission moves the atom to a center-of-mass state closer to the surface while phonon absorption changes the atomic state in the opposite direction (see Figs. 1 and 2). Our results for the rates are in good qualitative agreement with the results of Oria *et al.*, albeit with the Morse potential [5]. We stress that we include a large number of vibrational levels as a consequence of the deep silica-cesium potential. Note that the earlier work on this theme involved much fewer levels [5].

We next study the effect of temperature on the decay rates. The results for the phonon-mediated decay rates for $T=30$ K are shown in Fig. 7. In contrast to Fig. 6, the absorption rate is now much smaller than the corresponding emission rate for both shallow and deep levels. Thus, while it is difficult to distinguish the two log-scale curves for deep and shallow levels at room temperature (see Fig. 6), they are well resolved at low temperature (see Fig. 7).

B. Transitions from free states

We now calculate the rates for transitions from free states to other levels. We first examine free-to-bound transitions, which correspond to the adsorption process. According to Eq. (43), the free-to-bound (more exactly, quasicontinuum-to-bound) transition rate $G_{\nu f}$ depends not only on the continuum-to-bound transition rate density $R_{\nu f}$ but also on

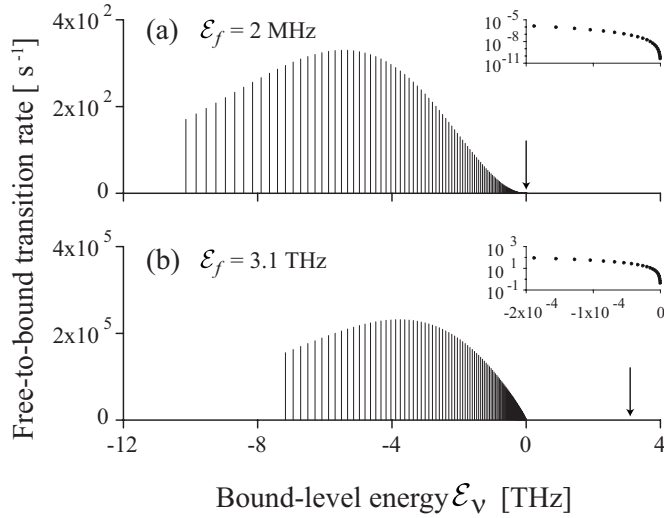


FIG. 8. Free-to-bound transition rates G_{vf} for transitions from the free plane-wave states with energies (a) $\mathcal{E}_f = 2$ MHz and (b) $\mathcal{E}_f = 3.1$ THz to bound levels ν as functions of the bound-level energy \mathcal{E}_ν . The arrows mark the energies of the initial free states. The insets show G_{vf} on the log scale versus \mathcal{E}_ν in the range from -200 MHz to -0.2 MHz to highlight the rates to shallow bound levels. The length of the free-atom quantization box is $L = 1$ mm. The temperature of the phonon bath is $T = 300$ K. Other parameters are as in Fig. 3.

the length L of the free-atom quantization box. To be specific, we use in our numerical calculations the value $L = 1$ mm, which is a typical size of atomic clouds in magneto-optical traps [19].

We plot in Fig. 8 the free-to-bound transition rate G_{vf} [see Eq. (43)] as a function of the vibrational quantum number ν . The upper (lower) part of the figure corresponds to the case of the initial-state energy $\mathcal{E}_f = 2$ MHz ($\mathcal{E}_f = 3.1$ THz), which is close to the average kinetic energy per atom in an ideal gas with temperature $T_0 = 200$ μ K ($T_0 = 300$ K). We observe that the free-to-bound transition rate first increases and then decreases with increasing transition frequency $\omega_{f\nu} = (\mathcal{E}_f - \mathcal{E}_\nu)/\hbar$. Such behavior results from the competing effects of the mean phonon number, the phonon mode density, and the matrix element of the force, like in the case of bound-to-bound transitions (see Fig. 3). We also see a cutoff of the transition frequency, which is associated with the Debye frequency. Comparison of Figs. 8(a) and 8(b) shows that the transitions from low-energy free states have probabilities orders of magnitude smaller than those from high-energy free states. One of the reasons is that the transition rate G_{vf} is proportional to the velocity $v_f = (2\mathcal{E}_f/m)^{1/2}$ [see Eq. (43)]. The dependence of the transition rate density R_{vf} on the transition frequency $\omega_{f\nu}$ also plays an important role. Because of these reasons, the rates for the transitions from low-energy free states to shallow bound levels are very small [see the inset of Fig. 8(a)].

We show in Fig. 9 the free-to-bound decay rate G_f [see Eq. (44)], which is a characteristic of the adsorption process, as a function of the free-state energy \mathcal{E}_f . We see that G_f first increases and then decreases with increasing \mathcal{E}_f . The increase of G_f with increasing \mathcal{E}_f in the region of small \mathcal{E}_f (see the

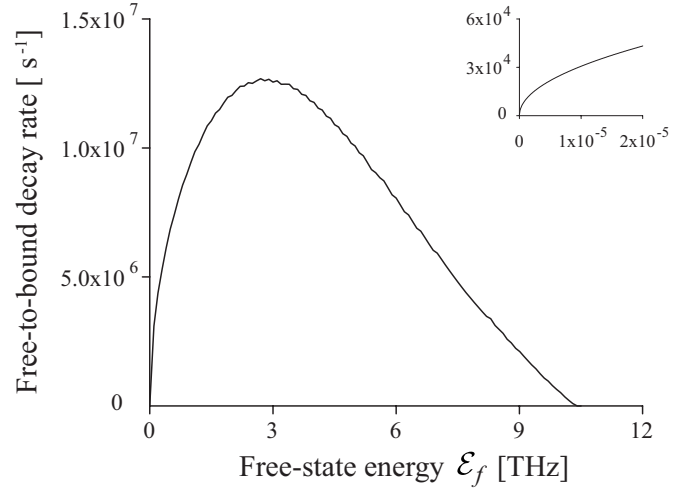


FIG. 9. Free-to-bound decay rate G_f as a function of the free-state energy \mathcal{E}_f . The inset highlights the magnitude and profile of the decay rate for \mathcal{E}_f in the range from 0 to 20 MHz. The temperature of the phonon bath is $T = 300$ K. Other parameters are as in Fig. 8.

inset) is mainly due to the increase in the atomic incidence velocity v_f . In this region, we have $G_f \propto v_f \propto \sqrt{\mathcal{E}_f}$ [see Eqs. (43) and (44)]. For \mathcal{E}_f in the range from 0 to 20 MHz, which is typical for atoms in magneto-optical traps, the maximum value of G_f is on the order of 10^4 s^{-1} (see the inset of Fig. 9). Such free-to-bound (adsorption) rates are several orders of magnitude smaller than the bound-to-free (desorption) rates (see the dashed curve in Fig. 5). The decrease of G_f with increasing \mathcal{E}_f in the region of large \mathcal{E}_f is mainly due to the reduction of the atom-phonon coupling coefficients.

In a thermal gas, the adsorption process is characterized by the transition rate G_{vT_0} [see Eq. (46)] and the decay rate G_{T_0} [see Eq. (47)], which are the averages of the free-to-bound transition rate G_{vf} and the free-to-bound decay rate G_f , respectively, over the free-state energy distribution (45). We plot the free-to-bound transition rate G_{vT_0} and the free-to-bound decay rate G_{T_0} in Figs. 10 and 11, respectively. Comparison between Figs. 10(a) and 8(a) shows that the transition rates from low-temperature thermal states and low-energy free states look quite similar to each other. The reason is that the spread of the energy distribution is not substantial in the case of low temperatures. The spread of the energy distribution is however substantial in the case of high temperatures, leading to the softening of the cutoff frequency effect [compare Fig. 10(b) with Fig. 8(b)]. Figure 11 shows that the free-to-bound decay rate G_{T_0} first increases and then reduces with increasing atomic temperature T_0 . For T_0 in the range from 100 μ K to 400 μ K, which is typical for atoms in magneto-optical traps, the maximum value of G_{T_0} is on the order of 10^4 s^{-1} [see Fig. 11(a)]. Such free-to-bound (adsorption) rates are several orders of magnitude smaller than the bound-to-free (desorption) rates (see the dashed curve in Fig. 5). Figure 11(a) shows that, in the region of low atomic temperature T_0 , one has $G_{T_0} \propto \sqrt{T_0}$, in agreement with the asymptotic behavior of Eqs. (46) and (47).

We now examine free-to-free transitions, both upward and downward, which correspond to the heating and cooling pro-

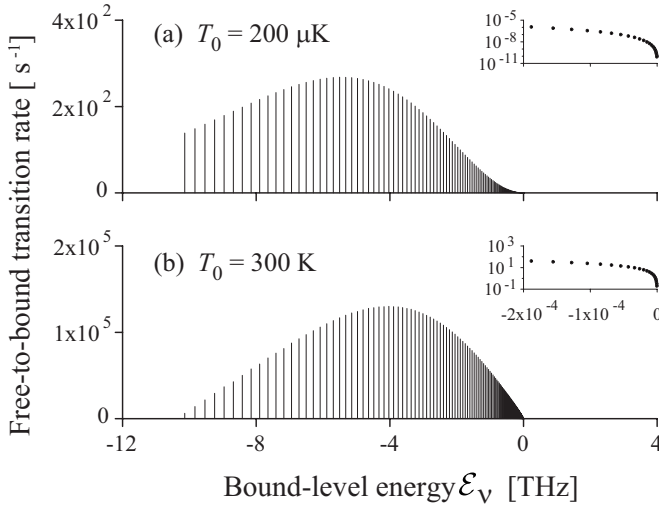


FIG. 10. Free-to-bound transition rates $G_{\nu T_0}$ for transitions from the thermal states with temperatures (a) $T_0=200 \mu\text{K}$ and (b) $T_0=300 \text{ K}$ to bound levels ν as functions of the bound-level energy \mathcal{E}_ν . The insets show $G_{\nu T_0}$ on the log scale versus \mathcal{E}_ν in the range from -200 MHz to -0.2 MHz to highlight the rates to shallow bound levels. The temperature of the phonon bath is $T=300 \text{ K}$. Other parameters are as in Fig. 8.

cesses of free atoms by the surface. We plot in Fig. 12 the free-to-free transition rate density $Q_{f'f}$ [see Eq. (48)] as a function of the final-level energy $\mathcal{E}_{f'}$. The upper (lower) part of the figure corresponds to the case of the initial-state energy $\mathcal{E}_f=2 \text{ MHz}$ ($\mathcal{E}_f=3.1 \text{ THz}$), which is close to the average kinetic energy per atom in an ideal gas with temperature $T_0=200 \mu\text{K}$ ($T_0=300 \text{ K}$). The rate densities are shown for the upward (phonon-absorption) and downward (phonon-emission) transitions by the solid and dashed lines, respectively. The figure shows that the free-to-free transition rate density increases or decreases with increasing transition frequency if the latter is not too large or is large enough, respectively. We also observe a signature of the Debye cutoff of the phonon frequency. Comparison of Figs. 12(a) and 12(b) shows that transitions from low-energy free states have

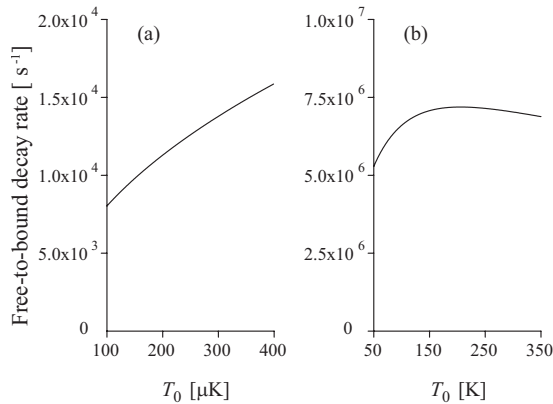


FIG. 11. Free-to-bound decay rate G_{T_0} as a function of the atomic temperature T_0 in the ranges (a) from $100 \mu\text{K}$ to $400 \mu\text{K}$ and (b) from 50 K to 350 K . The temperature of the phonon bath is $T=300 \text{ K}$. Other parameters are as in Fig. 8.

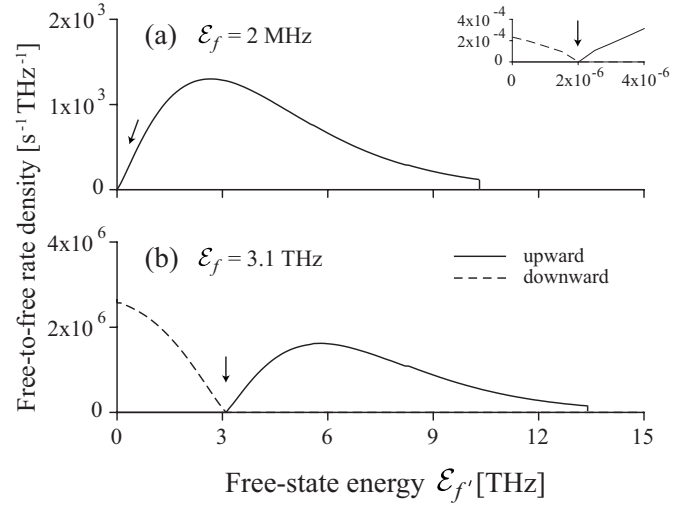


FIG. 12. Free-to-free transition rate densities $Q_{f'f}$ for the upward (solid lines) and downward (dashed lines) transitions from the free states $|f\rangle$ with energies (a) $\mathcal{E}_f=2 \text{ MHz}$ and (b) $\mathcal{E}_f=3.1 \text{ THz}$ to other free states $|f'\rangle$ as functions of the final-level energy $\mathcal{E}_{f'}$. The arrows mark the energies of the initial free states. The inset in part (a) shows $Q_{f'f}$ versus $\mathcal{E}_{f'}$ in the range from 0 to 4 MHz to highlight the small magnitude of the rate density for downward transitions (dashed line). The temperature of the phonon bath is $T=300 \text{ K}$. Other parameters are as in Fig. 8.

probabilities orders of magnitude smaller than those from high-energy free states. Figure 12(a) and its inset show that, when the energy of the free state is low, the free-to-free downward (cooling) transition rate is very small as compared to the free-to-free upward (heating) transition rate.

We show in Fig. 13 the free-to-free upward (phonon-absorption) and downward (phonon-emission) decay rates Q_f^a [see Eq. (50)] and Q_f^e [see Eq. (49)] as functions of the free-

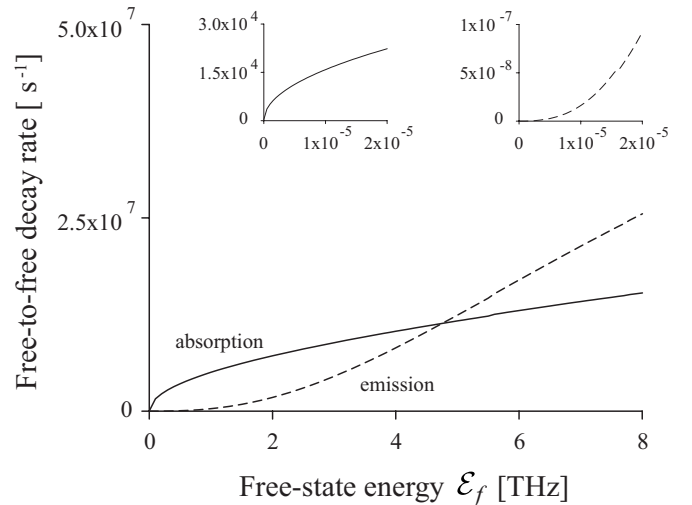


FIG. 13. Free-to-free upward and downward decay rates Q_f^a (solid lines) and Q_f^e (dashed lines) as functions of the energy \mathcal{E}_f of the initial free state. The insets highlight the magnitudes and profiles of the decay rates for \mathcal{E}_f in the range from 0 to 20 MHz . The temperature of the phonon bath is $T=300 \text{ K}$. Other parameters are as in Fig. 8.

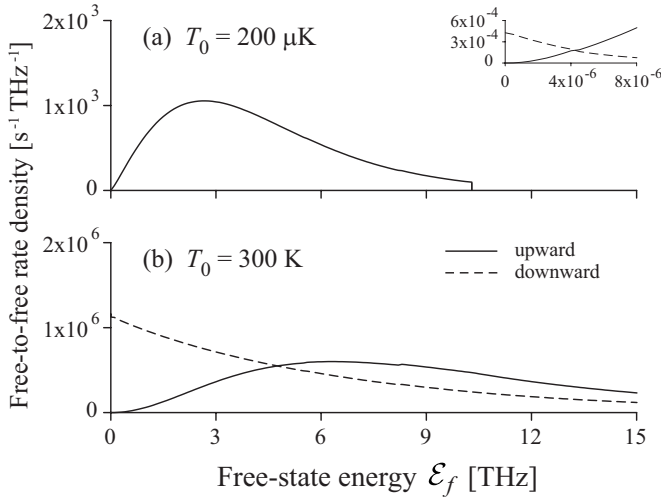


FIG. 14. Free-to-free transition rate densities $Q_{fT_0}^a$ for upward transitions (solid lines) and $Q_{fT_0}^e$ for downward transitions (dashed lines) from the thermal states with temperatures (a) $T_0=200\ \mu\text{K}$ and (b) $T_0=300\ \text{K}$ to free levels f as functions of the free-level energy \mathcal{E}_f . The inset in part (a) shows the rate densities versus \mathcal{E}_f in the range from 0 to 8 MHz to highlight the small magnitude of $Q_{fT_0}^e$ (dashed line). The temperature of the phonon bath is $T=300\ \text{K}$. Other parameters are as in Fig. 8.

state energy \mathcal{E}_f . We observe that Q_f^a and Q_f^e increase with increasing \mathcal{E}_f in the range from 0 to 8 THz. The increase of Q_f^a with increasing \mathcal{E}_f in the region of small \mathcal{E}_f (see the left inset) is mainly due to the increase in the atomic incidence velocity v_f . In this region, we have $Q_f^a \propto v_f \propto \sqrt{\mathcal{E}_f}$ [see Eqs. (48) and (50)]. The increase of Q_f^e with increasing \mathcal{E}_f in the region of small \mathcal{E}_f (see the right inset) is due to not only the increase in the atomic incidence velocity v_f [see Eq. (48)] but also the increase of the transition rate density Q_{ff}^e and the increase of the integration interval $(0, \mathcal{E}_f)$ [see Eq. (49)]. In this region, the dependence of Q_f^e on the energy \mathcal{E}_f is of higher order than $\mathcal{E}_f^{3/2}$. The left inset of Fig. 13 shows that, for \mathcal{E}_f in the range from 0 to 20 MHz, the maximum value of Q_f^a is on the order of $10^4\ \text{s}^{-1}$. Such free-to-free upward (heating) decay rates are comparable to but about two times smaller than the corresponding free-to-bound (adsorption) decay rates (see the inset of Fig. 9). Meanwhile, the right inset of Fig. 13 shows that, in the region of small \mathcal{E}_f , the free-to-free downward (cooling) decay rate Q_f^e is very small.

In the case of a thermal gas, the phonon-mediated heat transfer between the gas and the surface is characterized by the free-to-free transition rate densities $Q_{fT_0}^a$ and $Q_{fT_0}^e$ [see Eqs. (51)] and the free-to-free decay rates $Q_{T_0}^a$ and $Q_{T_0}^e$ [see Eqs. (52)]. We plot the free-to-free transition rate densities $Q_{fT_0}^a$ and $Q_{fT_0}^e$ in Fig. 14. Comparison between Figs. 14(a) and 12(a) shows that the transition rate densities from low-temperature thermal states and low-energy free states are quite similar to each other. The spread of the initial-state energy distribution is not substantial in this case. However, the energy spread of the initial state is substantial in the case of high temperatures, concealing the cutoff frequency effect [compare Fig. 14(b) with Fig. 12(b)]. We display the free-to-free decay rates $Q_{T_0}^a$ and $Q_{T_0}^e$ in Fig. 15. The solid and dashed

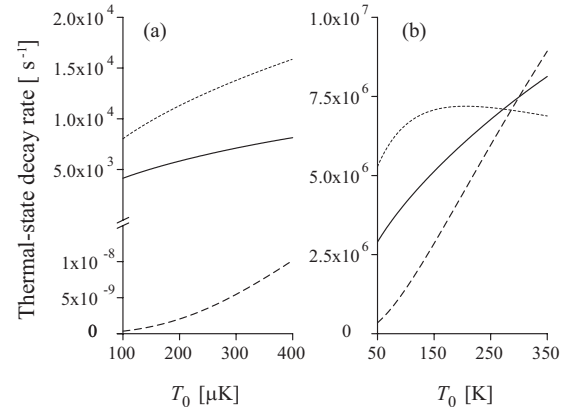


FIG. 15. Free-to-free decay rates $Q_{T_0}^a$ (solid lines) and $Q_{T_0}^e$ (dashed lines) for upward and downward transitions, respectively, as functions of the atomic temperature T_0 in the ranges (a) from $100\ \mu\text{K}$ to $400\ \mu\text{K}$ and (b) from $50\ \text{K}$ to $350\ \text{K}$. For comparison, the free-to-bound decay rate G_{T_0} is replotted from Fig. 11 by the dotted lines. The temperature of the phonon bath is $T=300\ \text{K}$. Other parameters are as in Fig. 8.

lines correspond to the upward (heating) and downward (cooling) transitions, respectively. For comparison, the free-to-bound decay rate (adsorption rate) G_{T_0} is replotted from Fig. 11 by the dotted lines. We observe that, for T_0 in the range from $100\ \mu\text{K}$ to $400\ \mu\text{K}$ [see Fig. 15(a)], the adsorption rate G_{T_0} (dotted line) is about two times larger than the heating rate $Q_{T_0}^a$ (solid line), while the cooling rate $Q_{T_0}^e$ (dashed line) is negligible. Figure 15(a) shows that, in the region of low atomic temperatures, one has $Q_{T_0}^e \cong Q_{T_0}^a \propto \sqrt{T_0}$, in agreement with the asymptotic behavior of expressions (52). The figure also shows that $Q_{T_0}^e$ quickly increases with increasing atomic temperature T_0 . The relation $Q_{T_0}^e < Q_{T_0}^a$, obtained for $T_0 < T$, indicates the dominance of heating of cold free atoms by the surface. The substantial magnitude of the free-to-bound transition rate G_{T_0} (dotted line) indicates that a significant number of atoms can be adsorbed by the surface. According to Fig. 15(b), the free-to-free downward transition rate $Q_{T_0}^e$ (dashed line) crosses the upward transition rate $Q_{T_0}^a$ (solid line) when $T_0=T=300\ \text{K}$, and then becomes the dominant decay rate. The relation $Q_{T_0}^e > Q_{T_0}^a$, obtained for $T_0 > T$, indicates the dominance of cooling of hot free atoms by the surface.

V. CONCLUSIONS

In conclusion, we have studied the phonon-mediated transitions of an atom in a surface-induced potential. We developed a general formalism, which is applicable for any surface-atom potential. A systematic derivation of the corresponding density-matrix equation enables us to investigate the dynamics of both diagonal and off-diagonal elements. We included a large number of vibrational levels originating from the deep silica-cesium potential. We calculated the transition and decay rates from both bound and free levels. We found that the rates of phonon-mediated transitions between

translational levels depend on the mean phonon number, the phonon mode density, and the matrix element of the force from the surface upon the atom. Due to the effects of these competing factors, the transition rates usually first increase and then reduce with increasing transition frequency. We focused on the transitions from bound states. Two specific examples, namely, when the initial level is a shallow level and also when it can be one of the deep levels, have been worked out. We have shown that there can be marked differences in the absorption and emission behavior in the two cases. For example, both the absorption and emission rates from the deep bound levels can be several orders (in our case, six orders) of magnitude larger than the corresponding rates from the shallow bound levels. We also analyzed various

types of transitions from free states. We have shown that, for thermal atomic cesium with temperature in the range from 100 μ K to 400 μ K in the vicinity of a silica surface with temperature of 300 K, the adsorption (free-to-bound decay) rate is about two times larger than the heating (free-to-free upward decay) rate, while the cooling (free-to-free downward decay) rate is negligible.

ACKNOWLEDGMENTS

We thank M. Chevrollier for fruitful discussions. This work was carried out under the 21st Century COE program on “Coherent Optical Science.”

-
- [1] V. I. Balykin, K. Hakuta, Fam Le Kien, J. Q. Liang, and M. Morinaga, Phys. Rev. A **70**, 011401(R) (2004); Fam Le Kien, V. I. Balykin, and K. Hakuta, *ibid.* **70**, 063403 (2004).
 - [2] Fam Le Kien, S. Dutta Gupta, V. I. Balykin, and K. Hakuta, Phys. Rev. A **72**, 032509 (2005).
 - [3] Fam Le Kien, S. Dutta Gupta, K. P. Nayak, and K. Hakuta, Phys. Rev. A **72**, 063815 (2005).
 - [4] E. G. Lima, M. Chevrollier, O. Di Lorenzo, P. C. Segundo, and M. Oriá, Phys. Rev. A **62**, 013410 (2000).
 - [5] T. Passerat de Silans, B. Farias, M. Oriá, and M. Chevrollier, Appl. Phys. B: Lasers Opt. **82**, 367 (2006).
 - [6] Fam Le Kien and K. Hakuta, Phys. Rev. A **75**, 013423 (2007).
 - [7] Fam Le Kien, S. Dutta Gupta, and K. Hakuta, Phys. Rev. A **75**, 032508 (2007).
 - [8] K. P. Nayak, P. N. Melentiev, M. Morinaga, Fam Le Kien, V. I. Balykin, and K. Hakuta, Opt. Express **15**, 5431 (2007).
 - [9] C. Henkel and M. Wilkens, Europhys. Lett. **47**, 414 (1999).
 - [10] Z. W. Gortel, H. J. Kreuzer, and R. Teshima, Phys. Rev. B **22**, 5655 (1980).
 - [11] H. Hoinkes, Rev. Mod. Phys. **52**, 933 (1980).
 - [12] See also *Interaction of Atoms and Molecules with Solid Surfaces*, edited by V. Bortolani, N. H. March, and M. P. Tosi (Plenum, New York, 1990); H. Lueth, *Surfaces and Interfaces of Solid Materials* (Springer, Berlin, 1997); A. V. Bogdanov, G. V. Dubrovskiy, M. P. Krutikov, D. V. Kulginov, and V. M. Strelchenya, *Interaction of Gases with Surfaces. Detailed Description of Elementary Processes and Kinetics* (Springer, Berlin, 1995).
 - [13] B. Bendow and S. C. Ying, Phys. Rev. B **7**, 622 (1973); S. C. Ying and B. Bendow, *ibid.* **7**, 637 (1973).
 - [14] N. N. Bogolubov, Commun. JINR Dubna **E17**, 11822 (1978); N. N. Bogolubov and N. N. Bogolubov, Jr., Elementary Particles and Nuclei (USSR) **11**, 245 (1980).
 - [15] R. Zwanzig, in *Lectures in Theoretical Physics*, edited by W. E. Brittin, B. W. Downs, and J. Downs (Interscience, New York, 1961), Vol. 3, p. 106; G. S. Agarwal, in *Progress in Optics*, edited by E. Wolf (North-Holland, Amsterdam, 1973), Vol. 11, p. 3; L. Mandel and E. Wolf, *Optical Coherence and Quantum Optics* (Cambridge, New York, 1995), p. 880.
 - [16] J. Javanainen and M. Mackie, Phys. Rev. A **58**, R789 (1998); M. Mackie and J. Javanainen, *ibid.* **60**, 3174 (1999).
 - [17] E. Luc-Koenig, M. Vatasescu, and F. Masnou-Seeuws, Eur. Phys. J. D **31**, 239 (2004).
 - [18] See, for example, G. P. Agrawal, *Nonlinear Fiber Optics* (Academic, New York, 2001).
 - [19] H. J. Metcalf and P. van der Straten, *Laser Cooling and Trapping* (Springer, New York, 1999).